J Mater Sci: Mater Med (2010) 21:1273–1287
DOI 10.1007/s10856-009-3939-2

Densification, phase stability and in vitro biocompatibility property of hydroxyapatite-10 wt% silver composites

Shekhar Nath · Sushma Kalmodia · Bikramjit Basu

Received: 6 September 2009 / Accepted: 6 November 2009 / Published online: 5 December 2009

Abstract In this paper, we demonstrate how a simple fabrication route, i.e., pressureless sintering of mechanically mixed powders can be employed to develop hydroxyapatite (HAp, $Ca_{10}(PO_4)_6(OH)_2$)-silver (Ag) bioceramic composites with superior combination of physical (hardness, toughness), non–cytotoxicity, cytocompatiblity and antimicrobial property. The densification results show that such composites can be sintered at 1200°C for 2 h near to theoretical density (>98% $\rho_{th)}$. An important observation is that the dissociation of HAp phase can be prevented during sintering up to 1300°C for 2 h in HAp-10 wt% Ag composites. The stability of HAp in presence of silver is discussed in reference to the results obtained using XRD, FTIR and Raman spectroscopy. The hardness values of the composites are comparable ($\sim$6.5 GPa) to that of pure HAp, despite of the presence of softer Ag particles. The sintered composites exhibit modest crack growth resistance property and their toughness varies in the range of 0.9–1.2 MPa $m^{0.5}$, depending on sintering temperature. For selected samples, the in vitro characterization was performed using mouse fibroblast (L929) and human osteosarcoma (MG63) cell lines. The combination of biochemical assays (MTT, ALP and osteocalcin) confirm that HAp-10 wt% Ag biocomposites have comparable or even better cellular viability, osteogenic differentiation and bone mineralization as well as osteoinduction property. Antibacterial experiments involving gram-negative bacteria, *Escherichia coli* confirm excellent bactericidal property of HAp-10 wt% Ag composites, sintered using mechanically mixed powders.

S. Nath · S. Kalmodia · B. Basu (✉)
Laboratory for Biomaterials, Department of Materials and Metallurgical Engineering, Indian Institute of Technology Kanpur, Kanpur 208016, UP, India
e-mail: bikram@iitk.ac.in

1 Introduction

Since last few decades, extensive research efforts have been being devoted to develop and characterize various biomaterials, based on ceramics, metals and polymer [1–8]. In particular, the biomaterials based on phosphate ceramics have received wider attention due to their excellent biocompatibility, when implanted in human/animal body. Of the many types of phosphate ceramics available, HAp and its composites have been extensively researched due to its structural and chemical similarity with bone mineral composition [9–11]. It is highly stable in body fluids and is known for its bioactivity, osteoinduction and osseoconductivity [12–14] i.e., it interacts with bone tissue upon implantation and enhances bone cell proliferation. Despite all such advantages, HAp has very poor mechanical properties and consequently, has limited application on its monolithic form. Therefore, metallic (Ag/Ti etc.) or ceramic (Al_2O_3, ZrO_2, mullite etc.) particulates are commonly incorporated in HAp matrix. An additional advantage with metallic reinforcement, like Ag is that Ag can potentially enhance the toughness and strength via ductile metal bridging mechanism [15, 16]. In addition to potential for improvement in mechanical properties, silver provides advantageous biochemical inertness and an antibacterial effect [17, 18]. Furthermore, high thermal expansion coefficient of silver (i.e., higher than HAp) implies that the HAp matrix, after cooling from sintering temperature, will be under residual compressive stresses and therefore, crack growth resistance can be improved to some extent. Zhang et al. [19] developed HAp-Ag composites from HAp and Ag_2O powder. They added variable amount of Ag (up to 30 vol.%) and sintered at 1250°C for 1 h. A good combination of strength and toughness of 80 MPa and 2.45 MP $m^{0.5}$ was achieved for 30 vol.% Ag, although the elastic modulus

was decreased on increasing silver addition. The main toughening mechanism was crack bridging and plastic work of Ag. Chaki and Wang [17] sintered HAp-10 wt% Ag composites in air at 1200°C for 1 h, culminating a densification of ~90% ρ_{th}. However, the densification was inferior to pure HAp (98% ρ_{th}). They achieved a flexural strength of ~75 MPa, which was superior to pure HAp (~39 MPa). In a different study, Lee et al. [20] reported the comparison in microstructure and fracture resistance property of HAp-5% Ag composites, fabricated using spark plasma sintering of electroless deposited powders. In all the above-mentioned studies, the biocompatibility property of the sintered composite was not evaluated.

Previous studies on silver modified HAp composites reported a moderate toughening mechanism in the material due to crack bridging [19]. As a shortcoming, the interface bonding between ceramic and metallic phase was found to be weak. Thus, no considerable plastic deformation of the silver particles was observed and the toughness of the composites was low. This problem has however been overcome using the HIP process [18]. The authors claimed that the new composites provided an enhancement of interfacial bonding between HAp and silver particles, leading to a tougher HAp based composite.

Feng et al. [21] studied the antimicrobial effect of Ag-HAp thin films on alumina substrate. They soaked the HAp coated alumina samples in $AgNO_3$ solutions, where the Ca^{2+} ions were substituted by Ag^{+} ions. Their results reveal that the $AgNO_3$ treated samples showed antimicrobial effect against different bacterial cells including Escherichia coli, Pseudomonas aeruginosa, Staphylococcus Aureus and Staphylococcus Epidermidis. However, the mechanical properties were not measured for such materials.

From the above, it must be clear that a comprehensive understanding of processing-microstructure—physical property—biological property correlation has not been achieved for HAp-Ag system. It needs to be pointed out that the biological properties are strongly sensitive to the chemistry or purity of HAp powders. Also, in many cases, either the physical properties or some important in vitro properties were not evaluated. In addition, the densification mechanism and its relation to hydroxyapatite stability during sintering are not clear. In view of this, the present paper analyzes HAp stability in presence of silver particle as well as reports how sintering conditions can influence microstructure development and hardness/toughness properties. In addition, the detailed in vitro experiments, such as cell adhesion, cell proliferation (MTT), bone cell differentiation (ALP, OC) are evaluated in order to explore the excellent capabilities of such materials to be successfully applicable in the field of biomedical applications.

2 Materials and method

2.1 Composite preparation

Hydroxyapatite was synthesized in house by well known suspension precipitation route [22, 23]. The precursor chemicals used in this synthesis, were calcium oxide (CaO) and phosphoric acid ($H_3(PO)_4$). Initially, CaO was dispersed in distilled water with a concentration of 18.6 g/l. The dispersed medium was kept on a hot plate and the suspension was stirred by an electric stirrer. Following this, an equivalent amount (keeping the Ca/P ratio same as HAp) of H_3PO_4 solution (0.17 M) was added drop wise in the dispersed CaO medium. The total solution was stirred at 80°C for 3–4 h to allow the reaction to take place towards completion. Then, concentrated NH_4OH (liquor ammonia) was added drop wise till the pH of the solution increases to 10. Subsequently, the solution was kept at room temperature for 1 day to precipitate the reaction product, which was collected with the help of a filter paper. The slurry was further dried at 100°C for 1 day. After drying, the lump was crushed by using an agate mortar to make the material in powder form. The dried powders were calcined at 800°C for 2 h, and the XRD peaks confirmed the pure hydroxyapatite phase. The calcined powders had the mean particle size, d_{50} of 1.3 μm (by laser particle size analyzer, model: Analysette 22; Fritsch GMBH, Germany). ICP-AES (Inductive coupled plasma-atomic emission spectroscopy: spectroflame modula FTM08, Germany) analysis using complexometry technique was performed to determine the Ca/P ratio of synthesized powder. A Ca/P atomic ratio of 1.64 was obtained with the HAp powder calcined at 800°C. It is important to note that, pure stoichiometric HAp possesses a Ca/P atomic ratio of 1.67. Therefore, the synthesized HAp powder was quite pure and stoichiometric. Commercially available silver powder was used in our study. 10 wt% Ag powder was mixed with HAp powder with the intention of synthesizing HAp-Ag particulate composites. Subsequently, the powder mixture was ball milled for 16 h in a planetary ball mill with acetone as milling medium. The balls and jar were made of agate and the weights of balls were seven times more than the weight of composite powders. Following this, the powder mixture slurry was dried and stored in glass bottle. Then, the composite powder was pressed uniaxially to form pellets of 12 mm diameter. These green pellets were then sintered in conventional sintering route in air atmosphere at the temperature range of 1000–1300°C for 2 h. The heating rate was maintained at 5°C/min and also the same rate has been followed up to 500°C during cooling. The sintering temperature has been optimized on the basis of sintered bulk density of the samples. The bulk density of all the sintered

samples were estimated by Archimedes' principle using distilled water as a fluid.

2.2 Characterizations of sintered samples

XRD analysis was carried out using CuK_{α} radiation to identify different phases present in the starting powders as well as in sintered materials. The dissociation behavior of HAp or formation of any reaction product was studied by critical analysis of XRD data. The microstructural observation of polished surface was made using SEM-EDS. All the smoothly polished samples were thermally etched at a temperature, 100°C lower than sintering temperature to reveal the grainy microstructure. The Fourier Transformed Infrared spectra (FT-IR, Vortex 70, BRUKER) were obtained in the range of 400–4000 cm^{-1} from the powder of various sintered samples at room temperature to confirm the presence of characteristic or functional bonds and groups. In addition, FT-IR data of KBr pellets were also obtained for comparison (dry run). To obtain the complementary information on stability of HAp, Raman spectra were also recorded with the argon ion laser, attached with Acton AM505F spectrometer in the wave number region of 1600–200 cm^{-1} and 3700–3100 cm^{-1} region at a laser power of 8 mW using an incident light with wavelength of 514.5 nm. The scattered radiation was collected at 180° (backscattering geometry) to the incoming beam and detected using a CCD cooled to −120°C.

To measure hardness, Vickers micro indents were taken on polished surface under 100 gm load. Hardness was measured by measuring the diagonal lengths of the indentations on SEM images. The hardness values were calculated using the following formula:

$$H_v = 1.854\left(\frac{P}{d^2}\right) \quad (1)$$

where H_v is Vickers hardness, P is the applied load; d is the average value of two diagonals.

Using indentation technique, the indentation toughness (K_{IC}) was estimated to assess the resistance to indent induced crack growth. It must be mentioned the precise measurements of crack length as well as the use of appropriate model/equation is important in the indentation toughness estimation for brittle materials. The choice of equation depends on the ratio of crack length (c) to indent diagonal (a). In the present case, the equation proposed by Niihara [24] is used, since c/a ratio is less than 3.5:

$$K_{IC} = 0.018Ha^{1/2}\left(\frac{E}{H}\right)^{2/5}\left(\frac{c}{a}-1\right)^{-1/2} \quad (2)$$

where K_{IC} = Fracture toughness, E = Elastic modulus, H = Hardness, c = 1/2 crack length, a = 1/2 diagonal length or d/2.

2.3 In vitro experiments

Mouse fibroblast (L929) and human osteosarcoma (MG63) cell lines were obtained from CCMB, Hyderabad and ATCC, respectively; and both cell lines were preserved in a LN_2 container. Prior to seeding on biomaterials surfaces, the cells were revived**.** In vitro cell adhesion property was evaluated for selected dense HAp-10Ag composites (sintered at 1200°C) using mouse fibroblast cells (L929) under scientifically controlled conditions. For comparison, similar study was done on pure HAp and negative control polymer disc. The first stage of sample preparation involved sterilization in order to remove other micro organisms, if present on the surface. Sterilization was done in an autoclave at 15 psi, 121°C for 20 min. The culture medium used for cell culture testing was DMEM (Dulbecco's modified Eagles' medium), containing 10% serum, 1% antibiotic cocktail. The samples were incubated for 48–72 h at 37.4°C (human body temperature). Subsequently, the cells were fixed using formaldehyde solution. Following this, the samples were prepared for SEM observation. This sample preparation involved replacement of PBS solution by adding a series of 30, 50, 70 and 100% ethyl alcohol solution. Afterwards, the samples were dried in a critical point dryer (CPD: Quramtech, UK) using liquid CO_2. The growth and proliferation of the fibroblast and osteoblast cells were subsequently observed using SEM.

For MTT analysis, after the incubation of 24 h, the medium was aspirated and samples were washed twice with PBS. 100 µl fresh DMEM was added (without phenol red). Subsequently, 10 µl reconstitute MTT (3(4,5-dimethylthiazol-2yl)-2-5diphenyltetrazolium bromide: SIGMA, USA, Cat No.M5655) was added in each well (5 mg/ml in DMEM culture medium without Phenol red and serum) and plate was incubated for 24 h. After the incubation period (8 h), the samples were removed from the well and 100 µl of DMSO (stop solution) was added in each well, including control. The culture plate was rocked for 1 h and the plate was left in the dark, overnight. The optical density of the solution was measured at 540 nm using ELISA automated microplate reader (Bio-Tek, ELx800).

The alkaline phosphatase (ALP) assay was used to examine cell differentiation such as osteogenesis, which is associated with increased expression of ALP. For the ALP assay, the autoclaved samples were placed in the four well plates and MG63 cells were seeded approximately at a density of 3×10^5/ml. After 2 days of culture, ascorbic

acid and vitamin D3 were added to activate the MG63 cell differentiation. The concentration of 1,25-dihydroxyvitamin D3 solution has significant effect of cell differentiation. The ALP activity experiments were conducted after 3rd and 7th days. The ALP, produced by the cells, was directly mixed with the culture solution. Therefore, after each time interval, the cells supernatant was used as the 'sample' for the test. The subsequent steps were followed as described in the commercial kit protocol (Alkaline Phosphatase, code no. 25904, Span Diagnostics Ltd., Surat, India) in a 96 well culture plate.

For the purpose of osteocalcin assay, human osteosarcoma (MG63) cells were cultured and seeded on HAp10Ag samples with negative control disc and pure HAp. The culture medium was replaced second day of culture. On day 2 and 5, vitamin D3 (10^{-8} M final concentration), ascorbic acid (50 μg/ml final) were added to the culture medium to enhance cell differentiation. To detect the amount of osteocalcin production by the metabolically active cells, three strips of coated wells were taken from the strips supplied with the osteocalcin kit (hOST-EASIA KAP1381, Biosource Europe S.A, Belgium). At 7th day, the sample surfaces were scrubbed with a scraper and the supernatant was used as 'sample' for the osteocalcin test. Thereafter, the osteocalcin experiment was carried out as per the protocol mentioned in the kit.

A bacterial cell line of *Escherichia coli* (*E.-coli,* ATCC #25922) was procured in the freeze dried condition from the American Type Culture Collection (ATCC). The bacteria cells were seeded on the samples (HAp-10Ag, control disc and pure HAp), allowed to adhere up to 4 h in an incubator at 37°C. Subsequently, the surface was rinsed twice with PBS and then soaked in primary fixative of 3% glutaraldehyde, 0.1 M sodium cacodylate, and 0.1 M sucrose, for 30 min. The surface was washed with buffer containing 0.1 M sodium cacodylate and 0.1 M sucrose for 5 min. The cells were dehydrated by replacing the buffer with ethanol series 30, 50, 70, 95, 100% for 10 min each and then further dried by critical point drier. The dried samples were sputter coated with a thin conductive coating of gold and examined under SEM.

2.4 Antimicrobial tests

A bacterial cell line of *Escherichia coli* (*E.-coli,* ATCC #25922) was procured in the freeze dried condition from the American Type Culture Collection. As a first step, the bacteria cell line was sub-cultured on a nutrient agar culture plate supplemented with 1% yeast extracts and trace elements. The bacteria were cultured on agar plates by streaking method and culture plate was incubated overnight at 37°C. Single bacterial colony was selected from culture plate using a sterile inoculation metal loop and inoculates in nutrient broth, a bacterial culture medium. Bacterial cells were incubated at 37°C and the cell density was adjusted approximately 10^6/ml in the suspension. Prior to seeding of bacteria, all the samples were ultrasonically cleaned and autoclaved. Subsequently, the samples were placed into culture dish and rinsed twice with PBS (1X). Three replicate samples from each composition were used for the experiment. The bacteria cells were seeded and allowed to adhere up to 4 h in an incubator at 37°C. Subsequently, after the incubation period, the surface was rinsed twice with PBS and then soaked in primary fixative of 3% glutaraldehyde, 0.1 M sodium cacodylate, and 0.1 M sucrose, for 30 min. The surface was washed with buffer containing 0.1 M sodium cacodylate and 0.1 M sucrose for 5 min. The cells were dehydrated by replacing the buffer with ethanol series 30, 50, 70, 95, 100% for 10 min each and then further dried by critical point drier. The dried samples were sputter coated with gold and examined under SEM.

3 Results

3.1 Densification and phase assemblages

Figure 1 plots the variation of densification with sintering temperature for pure HAp and HAp-10 wt% Ag. The theoretical density was calculated, assuming no silver reacted with HAp matrix. For pure HAp, the maximum densification ($\sim$98% ρ_{th}) reaches at 1200°C. On heating further, the densification reduces to a little extent. Like pure HAp, the maximum density for HAp10Ag samples reach at a peak

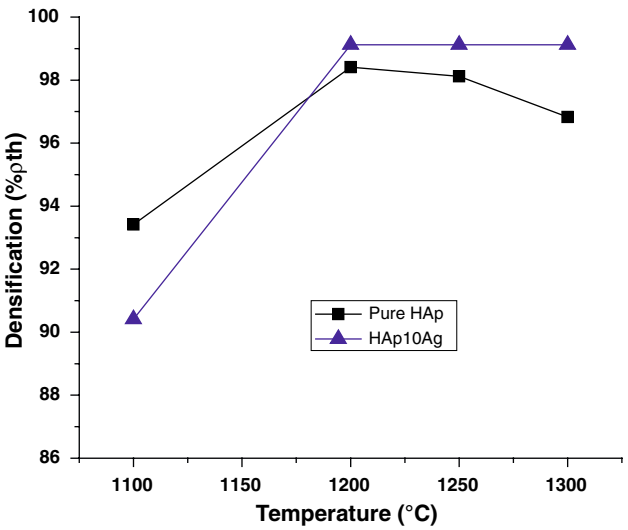

Fig. 1 Plot of densification (expressed as % theoretical density, ρth) versus sintering temperature for HAp monolith and HAp-10 wt% Ag composite. The theoretical density (ρ_{th}) was calculated assuming no reactions and dissociation of phases

value (~99% ρ_{th}), when sintered at 1200°C. It is to be noted here that sintering at a temperature higher than 1200°C does not have any effect on the densification. On the basis of densification data, it can be said that 10 wt% Ag addition does not degrade the densification behavior to any noticeable extent and the matrix densification dominates in the composite. This result is interesting as the dissociation of pure HAp occurs at a temperature of above 1200°C and therefore, density decreases noticeably above 1200°C. However, such behavior is not observed in case of HAp-10%A Ag, as no change in relative density is noticed during sintering at or up to 1300°C. This indicates that the presence of Ag can suppress the dissociation. It can be further mentioned that Lee et al. reports the dissociation of HAp to TCP in HA- 5 wt% Ag composites, when spark plasma sintered at 1000°C for 2 min [20].

Figure 2 presents XRD pattern of HAp-10Ag composites, sintered at various temperatures (1000–1300°C). For all the sintering temperatures, the dominant presence of HAp phase could be realized and the dissociation of HAp could not be observed till 1300°C. Also, the presence of silver phase was recorded in composites sintered up to 1250°C. In case of monolithic HAp, the dissociation to TCP phase was observed above 1200°C (not shown). The extreme stability of HAp against dissociation to TCP phase in composite will be explained in a subsequent section.

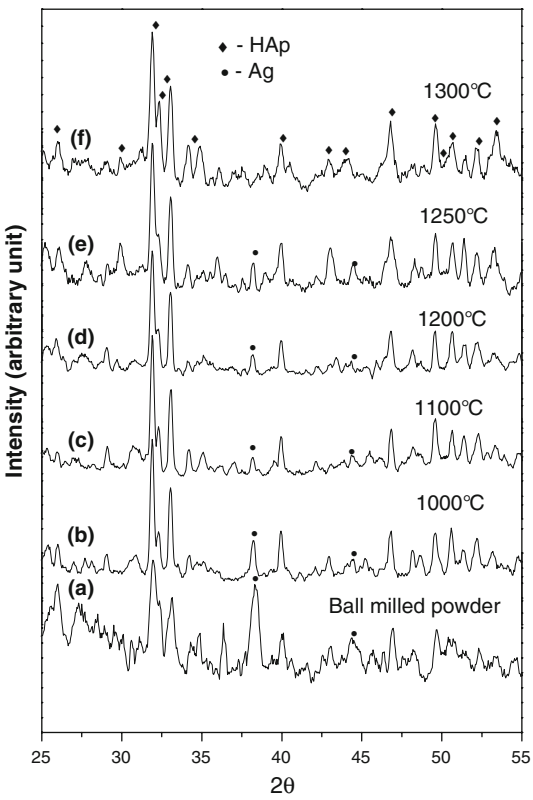

Fig. 2 Powder XRD spectra from HAp10Ag composites, sintered for 2 h at various temperatures: (*a*) ball-milled powder, (*b*) 1000°C, (*c*) 1100°C, (*d*) 1200°C, (*e*) 1250°C and (*f*) 1300°C

Figure 3 shows the FTIR results obtained from pure HAp and HAp-10Ag composites. For pure HAp (sintered at 1100°C), the presence of strong O–H vibration peak could be noticed at wave number of 3570 cm^{-1}. However, for HAp-10Ag samples, the intensity of O–H vibration peak is reduced, when sintered at 1100°C and even further reduced, when sintered at 1300°C. The presence of strong $-(PO_4)$ peaks are observed in all the cases. Complimentary information can be observed from the Raman spectroscopy data (Fig. 4). The presence of $-(PO_4)$ could be observed at wave numbers of 430 $cm^{-1}(v_2)$, 590 $cm^{-1}(v_4)$, 960 $cm^{-1}(v_1)$ and 1046 $cm^{-1}(v_3)$. In addition, the presence of O–H peak could be traced at 3570 cm^{-1} wave number.

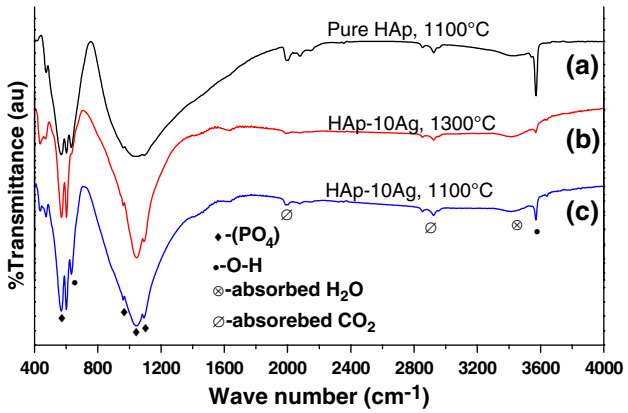

Fig. 3 Plots of FTIR spectra obtained from (*a*) pure HAp sintered at 1100°C for 2 h, (*b*) HAp-10Ag, sintered at 1300°C for 2 h, and (*c*) HAp-10Ag sintered at 1100°C for 2 h

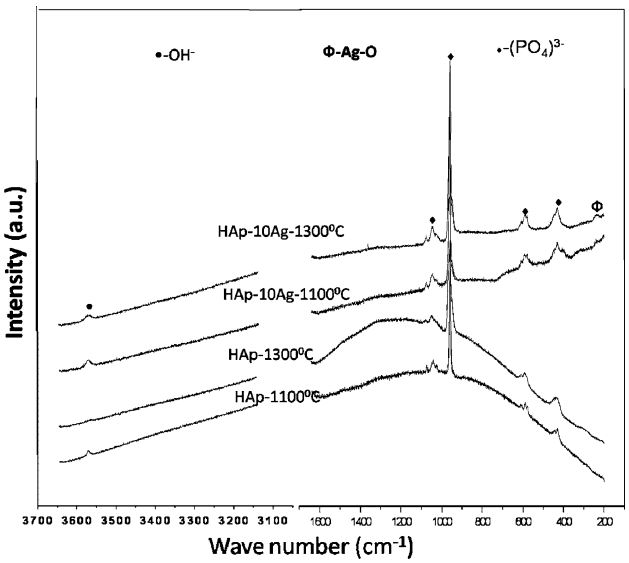

Fig. 4 Plots of Raman spectra obtained from pure HAp and HAp-10Ag, all are sintered for 2 h at various temperatures

Here, it needs to be pointed out that pure metallic silver is neither IR active nor Raman active and the formation of AgO and Ag_2O are not thermodynamically feasible up to the maximum sintering temperature (1300°C). The peaks of Ag–O bonding from AgO phase or Ag_2O phase could not be found in FTIR within its detection limit of 400–4000 cm^{-1} wave number. Therefore, except O–H stretching vibration peak (3570 cm^{-1} wavenumber), FTIR results do not show any difference, when Ag is added. If Ag diffuses in the HAp lattice then Ag–O vibration could be expected and the same was detected in Raman spectroscopy. The mechanism of dehydroxylation and Ag incorporation will be discussed in a subsequent section.

3.2 Microstructure observation

The microstructures of HAp-10 wt% Ag samples were observed on the polished and thermally etched samples using SEM. Figure 5 shows the microstructural features of HAp-10Ag samples sintered in the range of 1100–1300°C. At 1100°C (Fig. 5a), the microstructure is mainly characterized by homogeneous presence of porosity with fine grains of submicrometer sized. Here, the HAp and silver particles (bright contrast) could not be distinguished distinctively. However, with increasing sintering temperature to 1200°C, dense microstructure was observed (Fig. 5b). The bright contrast silver particles are dispersed throughout the matrix and in some cases; the particles appear to be agglomerated or clustered. Upon increasing sintering temperature at 1250°C, the microstructure is characterized by distinctly bimodal grains (Fig. 5c). In particular, the microstructure can be described by a few coarser HAp grains of 5–8 μm, dispersed in a fine grained matrix. Few intragranular pores can be observed at some locations. At 1300°C, the morphology of the silver particles is changed. A number of finer elongated Ag particles are found to disperse homogeneously throughout the grain boundary region. After sintering at 1300°C, the microstructure appears to be totally pore-free (Fig. 5d).

3.3 Mechanical properties

The basic mechanical properties, like hardness and indentation toughness were experimentally measured. In estimating toughness values, the theoretical E-modulus values of HAp-Ag composites were considered and the presence of porosity, was considered. Figure 6a plots the Vickers microhardness values of HAp-10 wt% Ag composites. The

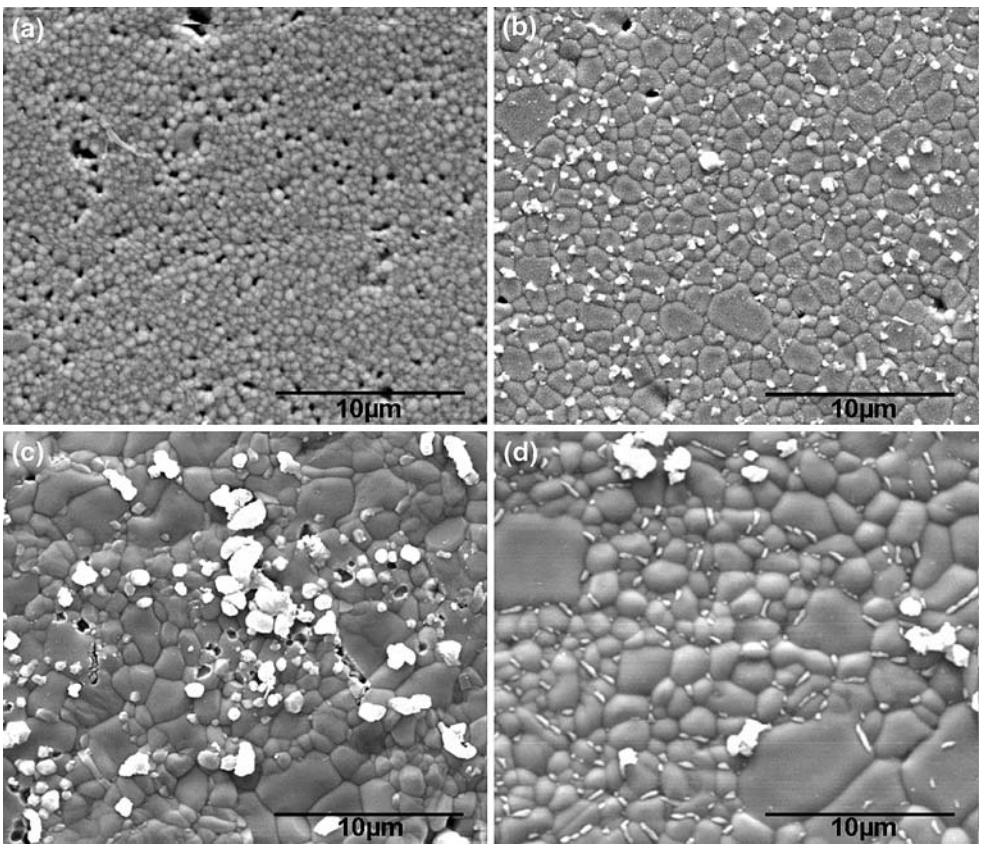

Fig. 5 SEM images of thermally etched HAp-10 wt% Ag composites, sintered at (**a**) 1100°C, (**b**) 1200°C, (**c**) 1250°C and (**d**) 1300°C

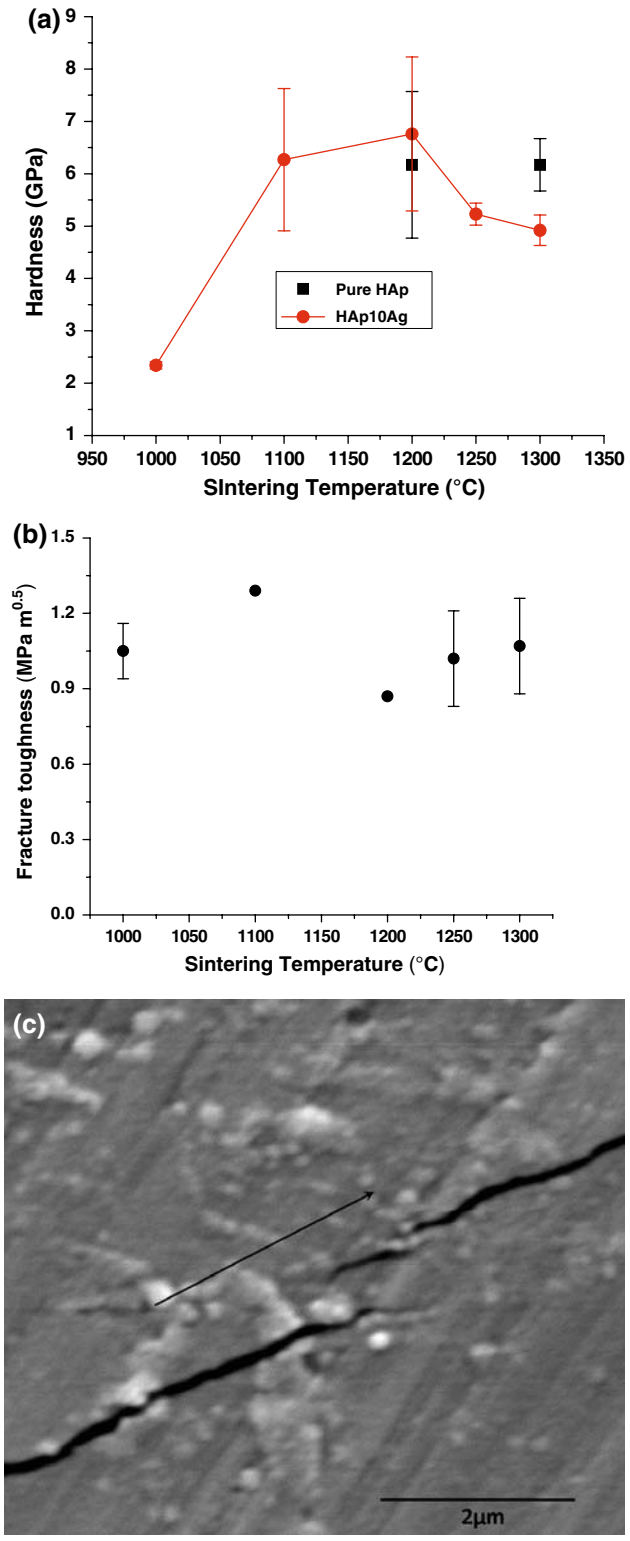

Fig. 6 Hardness (**a**) and fracture toughness (**b**) values of pure HAp and HAp-Ag composites (10 wt%), sintered at various temperatures, (**c**) indentation induced crack propagation, revealing crack branching around Ag particulates in HAp-10Ag composite sintered at 1250°C for 2 h

initial increase in hardness with increase in sintering temperature to 1100°C can be ascribed to better densification (see Fig. 1). Above 1200°C, a noticeable decrease in hardness from 6.7 to 5 GPa or less in HAp-10 wt% Ag samples (sintered at 1250 or 1300°C) was critically noted. Such a decrease in hardness can be correlated with the observation of the bimodal grain size, as reported in Fig. 5. The hardness of baseline HAp remains similar (~6 GPa) after sintering at 1200 or 1300°C. Overall, no significant difference in hardness property could be observed due to incorporation of 10 wt% Ag in HAp matrix.

In Fig. 6b, the indentation toughness values are plotted against sintering temperature. Overall, the toughness varies between 0.9 and 1.2 MPa $m^{0.5}$ and no clear correlation with processing condition was noticed. It can be noted here that no stable crack propagation could be found in case of pure HAp and in most cases, the indent induced damage/spalling was observed. In order to illustrate indent induced crack propagation behavior in HAp-10 wt% Ag, SEM image has been shown in Fig. 6c. The evidence of crack propagation through Ag particles or clusters is clear in Fig. 6c. The absence of any significant crack deflection correlates well with modest toughness value of the developed composite.

3.4 In vitro results

All the in vitro biocompatibility experiments were conducted on HAp-10 wt% Ag composite, sintered at 1200°C. Pure HAp (1200°C sintered) was chosen as baseline material and commercially available glass disc as control sample was used in our cell culture experiments. The samples were then autoclaved in a steam autoclave unit and were further used for the evaluation of in vitro properties. All the experimented samples were as sintered samples without any additional surface treatment. Therefore, the effect of surface roughness cannot explain any difference from sample to sample while evaluating in vitro properties.

In order to investigate cell adhesion behavior of composites, L929 mouse fibroblast cells were used. The reasons for using this particular cell line is that, (a) L929 cells can easily proliferate and adhere on most of the biomaterials surfaces, (b) L929 cells are the typical cell type, which participate in the early stage of wound healing process or any orthopedic fracture and (c) L929 cell line is widely used for preliminary biocompatibility evaluation for a wide range of biomaterials.

Some representative SEM images revealing cell adhesion behavior of HAp-10Ag composites, after culture with mouse fibroblast cell lines (L929) with cell density of

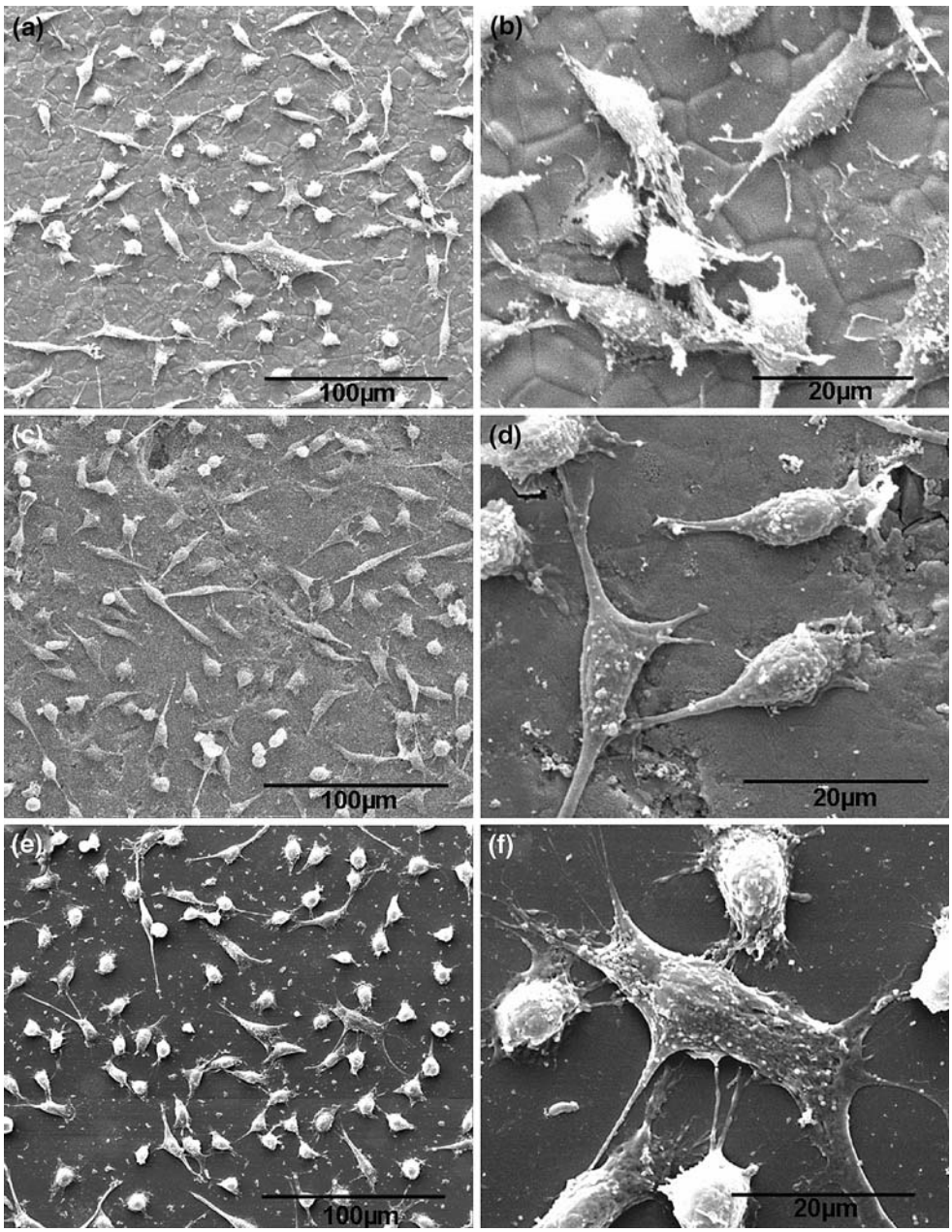

Fig. 7 SEM images of L929 cells adhered on pure HAp, sintered at 1200°C (**a**, **b**), HAp-10Ag, sintered at 1200°C for 2 h (**c**, **d**) and negative control samples (**e**, **f**). Results were obtained after 48 h of culture. The seeded cell density was 5×10^5 cells/ml

5×10^5/ml for 48 h are presented in Fig. 7. Figures 7a and b represent pure HAp surfaces, where as Figs. 7(c, d) and (e, f) show the cell adhesion on HAp-10Ag and control samples, respectively. The cell adhesion of the composite is comparable to pure HAp and control glass disc. In all cases, the common observation is cell-to cell contact, cell flattening and the long filopodia extension. In particular, the cells are spread across a number of grains in pure HAp, while extensive spreading on the HAp-10Ag often leads to Y-junction type feature. Overall, the cell spreading and adhesion of Ag containing HAp is comparable with that of pure Hap and no visible signature of cell apoptosis due to possible toxic effect of Ag addition could be noticed in Figs. 7c and d.

Some interesting features of cell adhesion were recorded, when cultured for 72 h with L929 cells with cell density of 1×10^5/ml (see Fig. 8). Figure 8a shows extreme flattening of cells with multiple filopodia, extended from all the directions of the cell surface. Figure 8b shows the contact between two flattened cells on the composite surface. Figure 8c reveals a large cell, spreading across a cluster of Ag particles. The EDS spectrum in the inset confirms that bright contrasting particles are Ag. The high magnification image in Fig. 8d shows that the

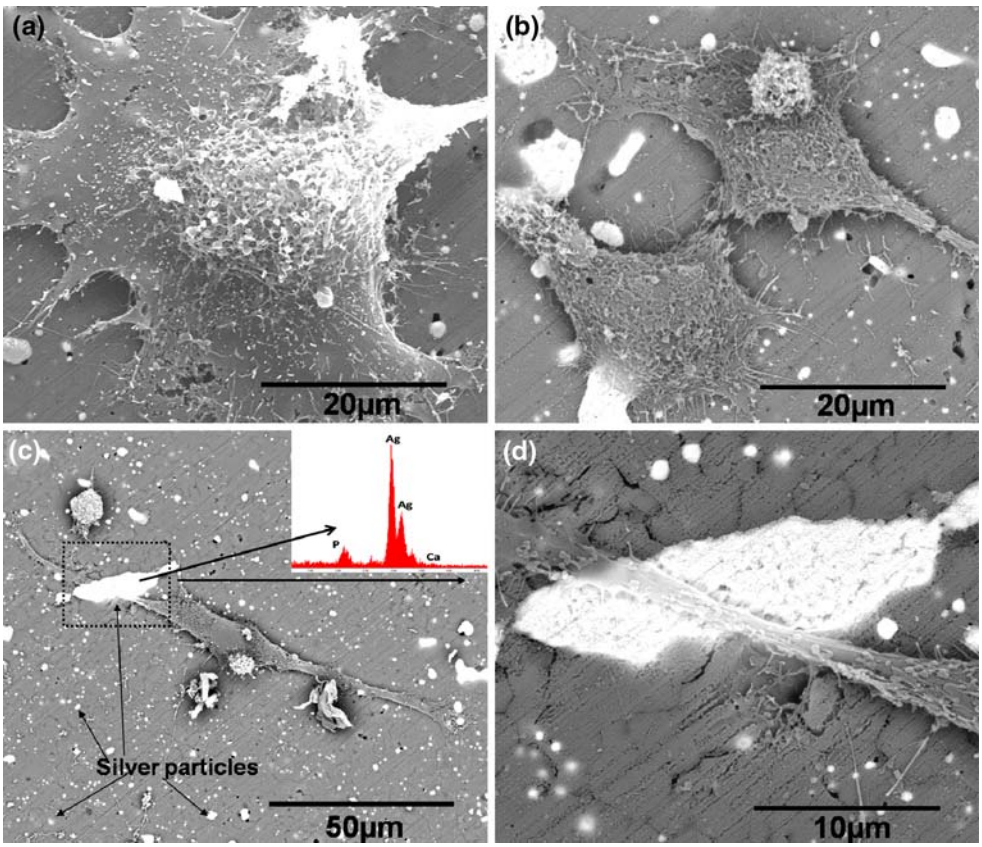

Fig. 8 SEM images of L929 cells adhered on HAp-10Ag (sintered at 1200°C) reveal the morphology of adhered cells. The white particles in the BSE images (**b**, **c**, and **d**) are silver particles. **c** and **d** reveal the cell adhesion in presence of silver. Results were obtained after 72 h of culture. The seeded cell density was 1×10^5 cells/ml

filopodia is thinner in contact with silver particles. Also, the lamelopodia are absent in the silver contact zone.

It is known that MTT reagent directly reacts with the mitochondria (Mitochondrial dehydrogenase) of living cells. Therefore, the reaction of MTT will be more if more number of metabolically active cells are present. Hence, MTT is widely regarded as one of the quantitative assays to determine the cytotoxicity of the materials, detecting the cell viability/proliferation on the sample surface. The measured optical density, as recorded with ELISA plate reader is directly proportional to the number of viable cells in the culture medium. Figure 9a plots the quantified data on cell proliferation using MTT assay. The results show that cell proliferation on HAp-10 wt% Ag composite is comparable with pure HAp. Due to the overlapping of error bars, no statistically significant difference in terms of Ag addition to HAp on cell viability can be confirmed using MTT results.

The bone cell functionality (differentiation) of such composites was evaluated using human osteosarcoma (MG 63) cell lines by alkaline phosphates and osteocalcin assay. The ALP assay indicates the initial stage bone mineralization capability of the material, whereas osteocalcin results reveal the later stage bone cell differentiation. As parameters for osteoinductive potential of the investigated biomaterial, the cell behavior is evaluated on their expression levels of ALP. Figure 9b shows the ALP test results of HAp 10Ag composites. From the plot, it is clear that the ALP activity is higher at day 3, compared to day 7 for both HAp and composites. Also, the ALP release is comparable for both the samples. Although marginally higher ALP expression of HAp-10Ag can be observed after 3 days, noticeably lower ALP expression of HAp-10Ag was recorded after 7 days, in reference to pure HAp.

It is normally accepted that the osteocalcin production measurement is important to substantiate the use of investigated ceramics as bone replacement materials. In terms of osteocalcin production, Hap-10Ag exhibits enhanced expression compared to pure HAp and control glass disc (Fig. 10). In view of the error bars being widely apart, such difference can be said to be statistically significant. Therefore, the osteocalcin production was increased in the presence of silver. Figure 11 shows the antimicrobial activity of 10 wt% Ag containing HAp composites after 4 h of inoculation. The results are compared with pure HAp (base line material) and polymer

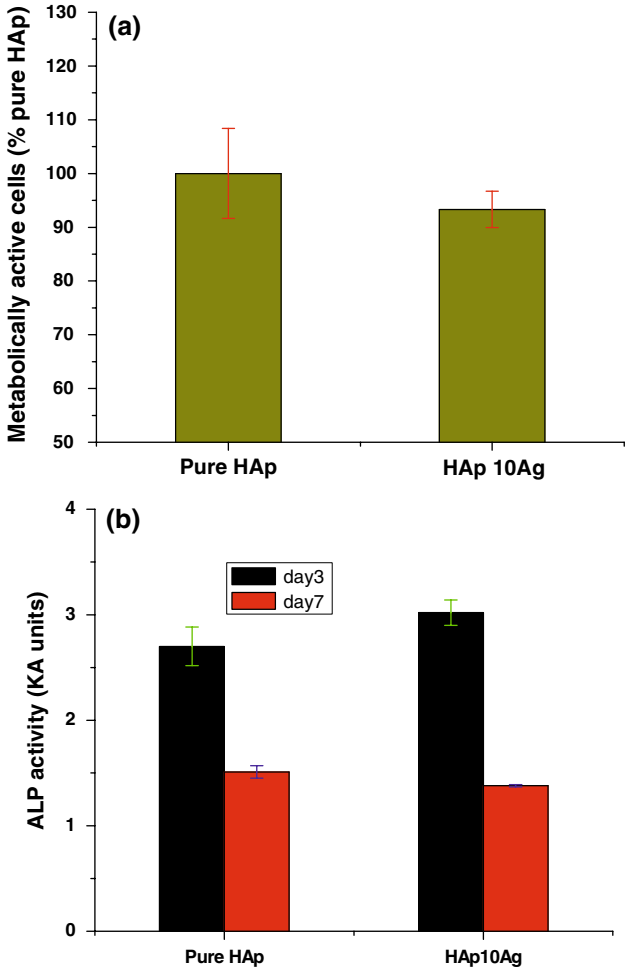

Fig. 9 **a** MTT assay results showing the relative number of metabolically active Mouse fibroblast cells (L929) proliferated on pure HAp (sintered at 1200°C) HAp-10 wt% Ag composite (sintered at 1200°C) and HAp 10Ag samples. The results are shown after 2 days of culture, **b** alkaline phosphatase activity (ALP) of HAp-Ag samples (sintered at 1200°C), showing ALP release from the cells after 3 and 7 days of culture. The results of pure HAp (sintered at 1200°C) are also represented for comparison

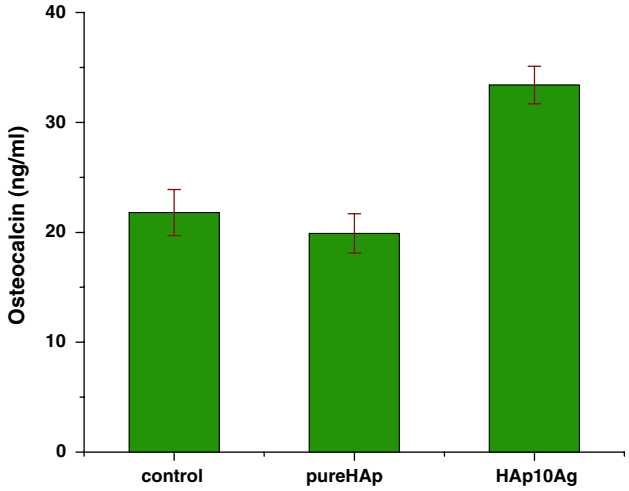

Fig. 10 Osteocalcin production of HAp-10 wt% Ag composite from the cultured MG63 cell lines after 7 days of culture. The results are compared with control solution supplied with the kit. Pure HAp (sintered at 1200°C) is represented as base line material

control disc. While longer aspect ratio E. coli bacteria largely adhere to HAp and strong clustering is observed on control disc, all the bacterial cells are killed on Ag containing sample. Comparing Fig. 11a,b and c, it is very clear that 10 wt% Ag is sufficient to induce bactericidal property against E-coli microorganisms.

4 Discussion

As presented in the last section, the experimental results of the present study demonstrate that 10% Ag addition to HAp has noticeable influence on the densification, phase stability as well as biological response in reference to that of pure HAp. To evaluate biological response as well as to assess whether the investigated material can support the attachment and proliferation of bone cells, both qualitative and quantitative results using cell adhesion test and various biochemical assays (MTT, ALP, Ostocalcin) results are obtained and analyzed in previous section. In the following, results will be interpreted in terms of influence of Ag addition on densification, phase stability, physical and biological properties. Such interpretation will be helpful to realize the following aspects: (a) extreme phase stability of HAp against dissociation to TCP during high temperature sintering of HAp-10% Ag composition; (b) Osteoinduction property based on biocompatibility with MG 63 cell line, (c) Biomineralisation ability based on ALP and osteocalcin assay results and (d) extremely good bactericidal property of HAp-10% Ag biocomposite.

4.1 Densification, microstructure and phase stability

In this section, we will discuss the important aspects of densification, phase stability and mechanical properties of HAp-Ag composites. The densification of pure HAp reaches peak value ($\sim$98% ρth) at around 1200°C (Fig. 1). At temperatures higher than 1200°C, negligible change in densification is recorded and this can be attributed to the dissociation of HAp phase to lower density TCP phase. For pure HAp, the sintering mechanism is purely solid state sintering. When Ag is mechanically mixed with HAp and sintered at temperatures of higher than 1000°C, Ag melts at $\sim$960°C during sintering. However, Ag (bright contrast phase) has low wettability on HAp surface. Therefore, all the Ag melts reside at the triple point or at the grain boundary region in droplet form. This melt does not spread along the grain boundary region. Even in some cases, the

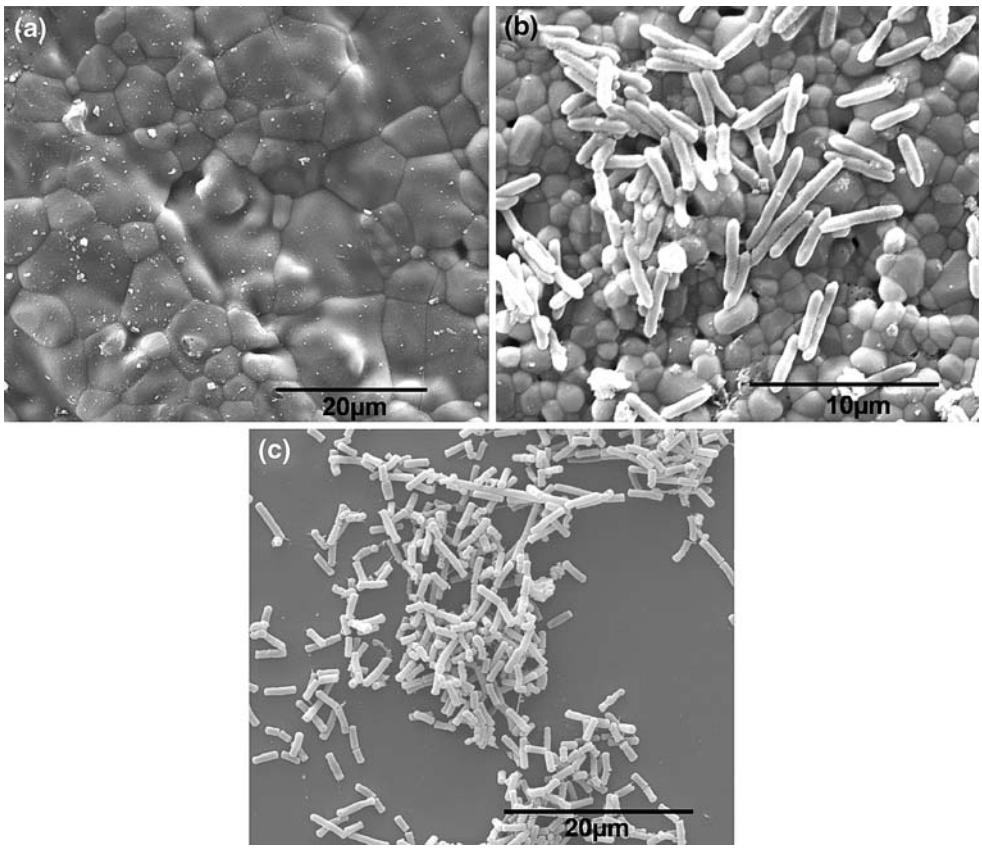

Fig. 11 SEM images revealing *E.-coli* bacterial cell adhesion on **a** HAp-10 wt% Ag composite (sintered at 1200°C), **b** pure HAp (sintered at 1200°C) and **c** negative control polymer disc after 4 h of inoculation

droplets are agglomerated and form bigger droplets (Fig. 5c). Due to such non-wetting behavior of Ag, the sintering mechanism is mainly driven by the solid state phenomenon even in the presence of liquid Ag. However, for HAp-10Ag composite, unlike pure HAp, the density remains unchanged in the temperature window of 1200–1300°C. The reason behind this result is that in presence of Ag, the stability of HAp increases and therefore, the formation of TCP is inhibited. XRD results support this phenomenon (Fig. 2). It can be noted here that the dissociation of HAp to TCP or sintering reactions takes place, when Ti or mullite is added to HAp and the powder mixture is pressureless sintered above 1000°C [9, 11].

In Fig. 3, the FTIR results show that the O–H vibration peak is getting reduced for HAp-10Ag composites, compared to pure HAp. Also with increasing sintering temperature, the O–H vibration is also reduced. Shirkhanzadeh et al. [25] could not find any extra peak in FTIR in the wave number range of 400–4000/cm after doping Ag in HAp lattice. Similar observation was reported by Lin et al. [26] in their work of Sr substituted HAp. They attributed the reduction of O–H peak intensity at 3570 wave number, on the weakening of O–H bond due to substitution of bigger Sr^{2+} ions. Therefore, it can be concluded that HAp does not dissociate and at the same time the O–H bond is modified in presence of Ag ion in the HAp unit cell lattice.

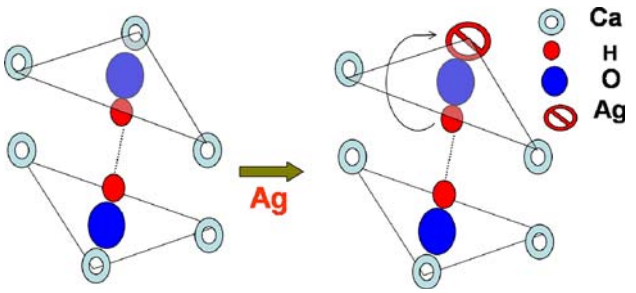

Fig. 12 Schematic illustration of incorporation of Ag ion in one of the Ca site in HAp unit cell

The diffusion of Ag in HAp lattice can be described by the following equation.

$$Ca_{10}(PO_4)_6(OH)_2 + 2xAg \xrightarrow{O} 2Ca_{10-x}Ag_{2x}(PO_4)_6 (OH)_2 + xCaO \quad (3)$$

The above equation indicates that Ag can be incorporated in HAp lattice and this is schematically shown in Fig. 12. Typically, the complex crystal structure of HAp is described by Ca triangle around OH column. In the presence of Ag, one of the Ca^{2+} sites can be substituted by Ag. Raman spectroscopy (Fig. 4) also confirms the presence of Ag–O bond [27] at 242 cm^{-1} wave number. It

is to be noted here that due to valency difference between Ca and Ag ions, a vacancy will be created in anion site, as per the following defect reaction:

$$2Ag \xrightarrow{Ca^{2+}} 2Ag'_{Ca} + V_O^{\circ\circ} \quad (4)$$

In the above equation, Kroger-Vink notation is adopted. From Fig. 12, it can therefore be perceived that the creation of oxygen vacancy will enable the proton of OH-bond to be attracted towards Ag-defect in the structure. Therefore, the stretching vibration of OH bond will be modified, as also observed in the FT-IR results (see Fig. 3).

An analysis of FT-IR results for natural bone mineral (HAp) shows substantial depletion or near-absence of O–H stretching vibration peak, although it was presumed that OH is present in crystal lattice of HAp. Cho et al. [28] confirmed the presence of OH in bone mineral using 2-D solid-state nuclear magnetic resonance (NMR) spectroscopy technique. Therefore, the absence of O–H stretching vibration indicates the interference of protein matrix. Similar absence of O–H peak was observed from the work of Jovanovic et al. [29] In their work, HAp was combined with polydimethylsiloxane (PDMS) water emulsion. It was reported that the absence of O–H stretching vibration peak at wave number of $\sim$3570 cm^{-1} is mainly due to the formation of hydrogen bond in between OH of HAp and OH/O of polymer chain. In the present case, a part of the available Ag melt could be evaporated at 1200°C or more and rest part could diffuse in HAp lattice and can replace the Ca^{2+} ions. Perhaps, due to the Ag incorporation in the lattice, the stability of HAp phase increases. It was already reported [30] that HAp can incorporate various metallic ions in its structure (Cd, Sr, Pb etc.). In the presence of these cations, the lattice parameter of HAp was observed to be changed.

In the present case, detectable peak shift for XRD peaks of HAp phase in composites is observed when compared to that in pure HAp. However, there is no detectable peak shift among the composites, which were sintered at various temperatures. This observation suggests that the extent of Ag diffusion had been reached at or before 1000°C. The lattice parameters of pure HAp in ball milled powder were calculated to be: a = 9.36632 ± 0.00382 A, c = 6.85744 ± 0.00571 A and unit cell volume, v = 520.991 ± 0.607 A^3. Whereas, the lattice parameters of HAp from the sintered composites were found to be: a = 9.38587 ± 0.00267 A, c = 6.85981 ± 0.00398 A and v = 523.349 ± 0.425 A^3. The calculations were done from the XRD data, using CellCalc software (HIROYUKI MIURA, Cellcalc version 1.51), considering hexagonal crystal structure with space group $P6_3/m$. From the calculated values, it is quite evident that the lattice parameters of HAp phase were changed when sintered with Ag particles. Both the 'a' and 'c' axes were increased slightly culminating increment in unit cell volume. The ionic radius of Ag^+ ion is 115 pm, whereas the ionic radius of Ca^{2+} is 100 pm. The above discussion indicates that larger Ag ions substitution in HAp lattice takes place during sintering of the composites.

As far as the mechanical properties are concerned, the present study shows that HAp-10 wt % Ag composites, if sintered at 1200°C, can exhibit high hardness of $\sim$6.5 GPa, which is comparable with pure HAp. However, the hardness values are sensitive to sintering temperature in case of HAp-10Ag composites, also mentioned in Sect. 3.2. Therefore, sintering temperature optimization is essential in tailoring microstructure and properties. However, the toughness does not show any strong dependency on sintering temperature or microstructure (see Figs. 5 and 6b). This is primarily due to extremely poor toughness of HAp matrix ($\sim$0.6 MPa $m^{0.5}$) and also lack of ductile metal bridging, as otherwise could be expected for metallic reinforcement. It is clear from the present results that Ag particulates, even up to 10 wt% addition, can not enhance toughness to any significant extent and therefore, additional toughening mechanisms need to be invoked to increase its toughness level to the lower bound of cortical bone toughness values ($\sim$3 MPa $m^{0.5}$).

4.2 Cytocompatibility, osteoinduction and bone mineralization property

In this section the in vitro biocompatibility of the investigated materials would be discussed on the basis of cell adhesion and cytocompatibility (MTT) and bone mineralization ability (ALP and osteocalcin assay). The results obtained with various in vitro experiments reflect that Ag incorporation (10 wt.%) in HAp matrix does not degrade overall biocompatibility of the composites. The back scattered SEM images in Fig. 8 shows the L929 cell and silver particle interaction, when the cell seeded density was 1×10^5 cells/ml. Figure 8a shows the cells are totally flattened, whereas Fig. 8b shows that contact between two cells. In Fig. 8b, c, and d, the bright particles are identified as Ag particles. Figure 8c shows the filopodia of a single cell going through a coarser Ag particle. A magnified image of Fig. 8c is presented in Fig. 8d. From closer observation of Fig. 8d, it could be observed that the filopodium of that cell is thinner, when it crosses the Ag particle. Freitas et al. [31] investigated cytotoxicity of silver amalgam in orthodontics. They showed that silver containing amalgam was toxic to fibroblast cell lines. However, in a separate study, Turner et al. [32] showed that silver coated cover slip did not show any cell adhesion (mouse 3T3 cells) though it was not toxic to the cells. Perhaps, the toxicity of amalgam persisted due to the presence of other metallic ions, such as copper and tin and not due to silver. The attachment of cells on the substrate

depends on the integrins, a transmembrane protein which connects the extracellular matrix (ECM) to the cellular actin cytoskeleton through focal adhesions [33, 34]. The non cell-adhesive properties of silver can be justified as it can inhibit thymidine during 'S' phase of cell proliferation [35]. On the other hand, the cell adhesion on the HAp particle region shows spreading of filopodium toward the substrate surface. As the amount of silver is less, the cell proliferation of the composites is similar to pure HAp. The quantitative assay (MTT) confirms this point firmly. From Fig. 9a, it is quite clear that the cell proliferation of the composite is $\sim$93% that of pure HAp.

As mentioned earlier, the aspects of osteoinduction and bone mineralization can be explained on the basis of ALP and osteocalcin assay results. It is well known that OC and ALP are the phenotypic markers of the late and early stages of differentiation of osteoblast-like cells, respectively. An increased specific activity of ALP in a bone cell population essentially reflects a shift to a more differentiated state i.e., reflects the differentiability of the progenitor bone cells in presence of specific materials or environments. Also, osteoinduction property essentially refers to the capability of promoting the differentiation of progenitor cells down an osteoblastic lineage. The cell differentiation or 'differential gene expression' is the process of spatial and temporal expression of a unique gene.

In the present context, some beneficial effect on cellular functionality could be understood from the ALP and Osteocalcin assay results. To determine the ALP and osteocalcin activities MG 63 (osteoblast like-cell) was used in presence of culture medium consisting ascorbic acid and vitamin $1,25(OH)_2D_3$. This vitamin activates osteoblast differentiation, whereas ascorbic acid plays a vital role in collagen synthesis and indirectly improves osteoblast differentiation.

The ALP activity results after 3 days, as presented in Fig. 9b, indicate that the composite can express marginally better bone-forming ability than pure HAp. Although after 7 days, the ALP expression is noticeably lower in composite than that in pure HAp. ALP activity is the initial bone formation marker and it depends on the attachment of alkaline phosphate on the cell membrane.

It is known that osteocalcin is a later stage marker of bone mineralization. Figure 10 shows that the osteocalcin production is statistically higher for HAp-10Ag composite, compared to control disc and pure HAp. Therefore, it could be inferred that Ag addition stimulate osteocalcin gene to promote bone mineralization. The presence of Ag is therefore expected to help in rapid bone ingrowths in vivo. Hardes et al. [36] compared osteoblast behavior of elementary silver versus titanium in vitro using human osteosarcoma (MG63) cell lines. They concluded that silver did not show toxicity and up to certain concentration limit; silver ions showed better osteogenic properties than titanium. However, further study is required to find out the detailed interaction of Ag ion with osteocalcin gene.

Summarizing, it can be said that the almost similar without much statistically significant difference in MTT and ALP expression of HAP-10% Ag in reference to pure HAp is due to the predominant presence of HAp in both the materials and the absence of TCP. In a recent work, it is confirmed that the presence of biphasic calcium phosphate microstructure containing varying ratio of HAp and TCP in case of HAp-Mullite can lead to better cell viability and osteogenicity compared to baseline HAp material. [37, 38] However, this aspect alone cannot explain higher osteocalcin expression of HAP-10% Ag composites.

4.3 Antimicrobial property

Another advantage of this developed composite is its antimicrobial properties. Figure 11 shows that after 4 h of inoculation HAp-Ag composite kill all the *E.-coli* bacteria. However, these bacteria survived and spread on the HAp and control samples. The mechanism of antimicrobial effect in presence of Ag has been already described in various earlier literatures [39–41]. The effectiveness of antimicrobial effect mainly depends on the Ag^+ release kinetics in the solution. Song et al. [42] reported that Ag caused plasmolysis i.e., cytoplasm of bacteria separated from bacterial cell wall. Egger et al. [43] speculated that, peptidoglycan, present in the bacterial cell wall contained teichoic acids or lipoteichoic acids which featured a strong negative charge, which might contributed to sequestering free Ag^{2+} ions. Rannie and barggs [44] demonstrated that silver ions could interact with sulfydryl (–SH) groups of proteins as well as the bases of DNA leading to the inhibition of respiratory processes. Batarseh [45] reported DNA unwinding in presence of Ag ions. From the above mentioned literature results it can be concluded that, the use of Ag could nullify the post operative infection after the implantation.

One of the major concerns in reference to HAp-Ag composites is that Ag addition, in an amount greater than a critical value just sufficient for anti-microbial property, can reduce cell proliferation. In an earlier study, Chen et al. [46] reported that antibacterial property in co-sputtered HAp-Ag composite coating required a minimum amount of 2.05 wt% Ag. In particular, Ag concentration of 10 mg/l has been reported [47] to cause a time-dependent depletion of intracellular ATP content of mammalian cells and thereby, causes necrosis [48]. Although Lee et al. [20] reported microstructure and fracture properties of HAp-5 wt% Ag composite; they did not carry out any biocompatibility test. In other studies [49–51], various researchers reported the antibacterial effect of Ag particles in HAp-Ag

coatings (synthesize by various routes), no detailed experimental investigation on cytocompatiblity was reported. From the present experimental results, it is clear that 10 wt% Ag does not induce any noticeable cytotoxicity effect and the bone cell differentiation as well bone mineralization ability of HAp-10Ag composite is comparable with that of pure HAp.

At the close, it can be stated that the present work demonstrates that the sintering of mechanically mixed powders of HAp and 10 wt% Ag can produce composites without dissociation of HAp. In addition, the composite materials also have comparable cellular functionality, in terms of cell viability, osteogenic expression, osteoinduction property like pure HAp.

5 Conclusions

Based on the experimental results of the present work, the following conclusions can be drawn:

a. The results of the sintering experiments reveal that the HAp-10 wt% Ag can be sintered to near theoretical density at 1200°C for 2 h in air and the solid state sintering mechanism of the HAp matrix appears to dominate the densification mechanism of the composite.
b. The combination of XRD, FT-IR and Raman spectroscopy results confirm the extreme stability of HAp phase against dissociation to TCP phases in HAp-10 wt% Ag composites during sintering up to 1300°C. The stability has been explained in terms of the incorporation of Ag into HAp lattice and a mechanism based on defect reactions as well as the formation of non-stoichiometric HAp has been proposed. The lattice parameters of HAp phase were changed due to Ag incorporation in the lattice.
c. Despite the addition of softer Ag particles, high hardness of around 6.5 GPa could be achieved in the HAp-10 wt% Ag composites, when sintered at 1200°C. However, a modest indentation toughness of around 1 MPa $m^{1/2}$ was measured and the crack branching was found to be the only toughening mechanism.
d. The results of the cell culture experiments with L929 mouse fibroblast cell line reveals that the addition of 10% Ag to HAp matrix does not cause any significant difference in the overall cell attachment, cellular bridge formation and cell proliferation behavior, in reference to pure HAp. Also, HAp-10% Ag favorably supports cell attachment and proliferation of L929 mouse fibroblast cells in vitro. As far as the quantification of the cytotoxicity is concerned, MTT assay results with fibroblast cells do not reveal any statistically significant variation in terms of metabolically active cells after culturing with the Ag containing composites in comparison with pure HAp.
e. The combination of ALP activity and OC expression results indicates that HAp-10 wt% Ag composites exhibit comparable/better bone cell differentiation and better bone mineralization property than baseline single phase HAp ceramic.
f. An important outcome of the present study is that the addition of 10% Ag can provide excellent anti-microbial property in terms of bactericidal property against *E. coli* bacteria without compromising on the in vitro cytocompatibility/cytotoxicity property of HAp.

Acknowledgment The authors express their gratitude for the financial support from Council of Scientific and Industrial Research (CSIR) and Department of Biotechnology (DBT), Government of India. The authors gratefully acknowledge Dr. Rajeev Gupta, Physics department, IIT Kanpur for his co-operation in allowing us to use the Raman spectroscopy unit.

References

1. Nath S, Basu B. Designing biomaterials for hard tissue replacement. J Kor Cer Soc. 2008;45:1–29.
2. Bodhak S, Nath S, Basu B. Understanding the fretting wear properties of HAp, Al_2O_3 containing HDPE biocomposites against ZrO_2. J Biomed Mat Res: Part A. 2008;85A:83–98.
3. Nath S, Bodhak S, Basu B. HDPE-Al_2O_3-HAp composites for biomedical applications: processing and characterization. J Biomed Mat Res: Part B Appl Biomat. 2009;88B:1–11.
4. Roy S, Basu B. On the development of two characteristically different crystal morphology in SiO_2–MgO–Al_2O_3–K_2O–B_2O_3–F glass-ceramic system. J Mat Sci: Mat Med. 2009;20:51–66.
5. Roy S, Basu B. *In vitro* dissolution behavior of SiO2–MgO–Al2O3–K2O–B2O3–F glass–ceramic system. J Mat Sci: Mat Med. 2008;19:3123–33.
6. Nath S, Bajaj S, Basu B. Microwave-sintered MgO-doped zirconia with improved mechanical and tribological properties. Int J App Ceram Tech. 2008;5:49–62.
7. Roy S, Basu B. Mechanical and tribological characterization of human tooth. Mater Charact. 2008;59:747–56.
8. Roy S, Basu B. Hardness properties and microscopic investigation of crack-crystal interaction in SiO_2–MgO–Al_2O_3–K_2O–B_2O_3–F glass ceramic system. Mater Sci Eng C. doi:10.1007/s10856-009-3853-7.
9. Nath S, Tripathi R, Basu B. Understanding phase stability, microstructure development and biocompatibility in calcium phosphate-titania composites, synthesized from hydroxyapatite and titanium powder mix. Mater Sci Eng C. 2009;29:97–107.
10. Nath S, Basu B, Mohanty M, Mohanan PV. *In vivo* response of novel hydroxyapatite-mullite composites: results up to 12 weeks of implantation. J Biomed Mat Res: Part B. 2009;90B:547–57.
11. Nath S, Biswas K, Basu B. TEM study of dissociation and thermochemical compatibility in HAp-mullite system. Scrip Mat. 2008;58:1054–7.
12. Hench LL. Bioceramics. J Am Ceram Soc. 1998;81:1705–28.
13. Ning CQ, Zhou Y. *In vitro* bioactivity of a biocomposite fabricated from HA and Ti powders by powder metallurgy method. Biomaterials. 2002;23:2909–15.

14. Jarcho M. Calcium phosphate ceramics as hard tissue prosthetics. Clin Orthop Rel Res. 1981;157:259–78.
15. Ducheyne P, Hench LL. The processing and static mechanical properties of metal fibre reinforced bioglass. J Mater Sci. 1982;17:595–606.
16. Zhang X, Gubbels GHM, Terpstra RA, Metselaar R. Toughening of calcium hydroxyapatite with silver particles. J Mater Sci. 1997;32:235–43.
17. Chaki TK, Wang PE. Densification and strengthening of silver-reinforced hydroxyapatite- matrix composite prepared by sintering. J Mater Sci: Mater Medicine. 1994;5:533–42.
18. Asmus SMF, Sakakuoorand S, Pezzotti G. Hydroxyapatite toughened by silver inclusions. J Comp Mat. 2003;37:2117–29.
19. Zhang X, Gubbels GHM, Terpestra RA, Metselaar R. Toughening of calcium hydroxyapatite with silver inclusions. J Mat Sci. 1997;32:235–43.
20. Lee BT, Shin NY, Han JK, Song HY. Microstructures and fracture characteristics of spark plasma-sintered HAp–5 vol% Ag composites. Mater Sci Eng: A. 2006;429:348–52.
21. Feng QL, Kim TN, Wu J, Park ES, Kim JO, Lim DY, et al. Antibacterial effects of Ag-HAp thin films on alumina substrates. Thin Sol Films. 1998;335:214–9.
22. Rathje W. Zur Kentnis de phosphate: I. Uber. Hydroxyapatite. Bodenk Pflernah. 1939;12:121–8.
23. Santos MH, Oliveira M, Souza LPF, Mansur HS, Vasconcelos WL. Synthesis control and characterization of hydroxyapatite prepared by wet precipitation process. Mater Res. 2004;7:625–30.
24. Niihara K, Morena R, Hasselman DPH. Evaluation of K_{Ic} of brittle solids by the indentation method with low crack-to-indent ratios. J Mater Sci Lett. 1982;1:13–6.
25. Shirkhanzadeh M, Azadegan M, Liu GQ. Bioactive delivery systems for the slow release of antibiotics: incorporation of Ag^{+} ions into micro-porous hydroxyapatite coatings. Mater Lett. 1995;24:7–12.
26. Yingguang L, Zhuoru Y, Jiang C, Lianshi W. Synthesis. Characterization and antibacterial property of strontium half and totally substituted hydroxyapatite nanoparticles. J Wuhan Univ Tech-Mater Sci Ed. 2008;23:475–9.
27. Morzyk-Ociepa B, Michalska D. Vibrational spectra of 1-methyluracilate complex with silver(I) and theoretical studies of the 1-MeU anion. Spectro Acta Part A. 2003;59:1247–54.
28. Cho G, Wu Y, Ackerman JL. Detection of hydroxyl ions in bone mineral by solid-state NMR spectroscopy. Science. 2003;300:1123–7.
29. Jovanovic J, Adnadjevic B, Kicanovic M, Uskokovic D. The influence of hydroxyapatite modification on the cross-linking of polydimethylsiloxane/HAp composites. Coll Surf B: Biоint. 2004;39:181–6.
30. Zhua K, Yanagisawa K, Shimanouchi R, Onda A, Kajiyoshi K. Preferential occupancy of metal ions in the hydroxyapatite solid solutions synthesized by hydrothermal method. J Euro Ceram Soc. 2006;26:509–13.
31. Freitas MPM, Oshima HMS, Menezes LM, Machado DC, Viezzer C. Cytotoxicity of silver solder employed in orthodontics. Angle Orthod. 2009;79:939–44.
32. Turner N, Armitage M, Butler R, Ireland G. An *in vitro* model to evaluate cell adhesion to metals used in implantation shows significant differences between palladium and gold or platinum. Cell Bio Int. 2004;28:541–7.
33. West KA, Zhang H, Brown MC. The LD4 motif of paxillin regulates cell spreading and motility through an interaction with paxillin kinase linker (PKL). J Cell Biol. 2001;154:161–76.
34. Misra A, Lim RPZ, Wu Z, Thanabalu T. N-WASP plays a critical role in fibroblast adhesion and spreading. Biochem Biophys Res Commun. 2007;364:908–12.
35. Syrjanen S, Hensten-Pettersen A, Kangasniemi K, Yli-Urpo A. In vitro and *in vivo* biological responses to some dentalalloys tested separately and in combinations. Biomaterials. 1995;7:169–76.
36. Hardes J, Streitburger A, Ahrens H, Nusselt T, Gebert C, Winkelmann W, Battmann A, Gosheger G. The influence of elementary silver versus titanium on osteoblasts behaviour *in vitro* using human osteosarcoma cell lines. Sarcoma. 2007. doi: 10.1155/2007/26539.
37. Nath S. Development of novel calcium phosphate-mullite composites for orthopedic application, PhD thesis, IIT Kanpur, September 2008.
38. Nath S, Kalmodia S, Basu B. Cytotoxicity and bone mineralization properties of novel calcium phosphate-mullite composites. J Biomed Mat Res: Part A (under review, 2009).
39. Matsumura Y, Yoshikata K, Kunisaki SI, Tsuschido T. Mode of bactericidal action of silver zeolite and its comparison with that of silver nitrate. Appl Environ Microbiol. 2003;69:4278–81.
40. Richards RME, Taylor RB, Xing DKL. Effect of silver on whole cells and speroplasts of a silver resistant pseudomonas aeruginosa. Microbios. 1984;39:151–8.
41. Russell AD, Hugo WB. Antimicrobial activity and action of silver. Prog Med Chem. 1994;31:351–71.
42. Song HY, Ko KK, Oh IH, Lee BT. Fabrication of silver nanoparticles and their antimicrobial mechanisms. Eur Cells Mater. 2006;11:58.
43. Egger S, Lehmann RP, Height MJ, Loessner MJ, Schuppler M. Antimicrobial properties of a novel silver-silica nanocomposite material. Appl Environ Microbiol. 2009;75:2973–6.
44. Bragg PD, Rannie DJ. The effect of silver ions on the respiratory chain of *E coli*. Can J Microbiol. 1974;20:883–9.
45. Batarseh KI. Anomaly and correlation of killing in the therapeutic properties of silver (I) chelation with glutamic and tartaric acids. J Antimicrob Chemother. 2004;54:546–8.
46. Chen W, Liu Y, Courtney HS, Bettenga M, Agrawal CM, Bumgardner JD, et al. *In vitro* anti-bacterial and biological properties of magnetron co-sputtered silver-containing hydroxyapatite coating. Biomaterials. 2006;27:5512–7.
47. Vik H, Andersen KJ, Julshamn K, Todnem K. Neuropathy caused by silver absorption from arthroplasty cement. Lancet. 1985;1:872.
48. Hidalgo E, Dominguez C. Study of cytotoxicity mechanisms of silver nitrate in human dermal fibroblasts. Toxicol Lett. 1998;98:169–79.
49. Feng QL, Kim TN, Wu J, Park ES, Kim JO, Lim DY, et al. Antibacterial effects of Ag-HAp thin films on alumina substrates. Thin Solid Films. 1998;335:214–9.
50. Lee IS, Whang CN, Oh KS, Park JC, Lee KY, Lee GH, et al. Formation of silver incorporated calcium phosphate film for medical applications. Nucl Instrum Methods Phys Res Sec B: Beam Interac Mat Atoms. 2006;242:45–7.
51. Shirkhanzadeh M, Azadegan M, Liu GQ. Bioactive delivery systems for the slow release of antibiotics: incorporation of Ag^{+} ions into micro-porous hydroxyapatite coatings. Mater Lett. 1995;24:7–12.